DC to Single-phase AC Grid-Tied Inverter using Buck Type Active Power Decoupling without additional magnetic component

Jun-ichi Itoh, Tomokazu Sakuraba, Hiroki Watanabe, Nagisa Takaoka
Nagaoka University of Technology
Department of Electrical, Electronics and Information
Nagaoka, Niigata, Japan
itoh@vos.nagaokaut.ac.jp, t_sakuraba@stn.nagaokaut.ac.jp, hwatanabe@stn.nagaokaut.ac.jp, ntakaoka@stn.nagaokaut.ac.jp

***Abstract*— This paper proposes a single-phase AC converter with an active power decoupling circuit operated in DCM (discontinuous current mode) for PV (photovoltaic) systems. The proposed converter consists of an H-bridge single-phase AC converter and a boost converter, and a compensation circuit employed with a small capacitor for the power ripple. In many active power decoupling topologies that have been studied, an additional magnetic component for the voltage control of the buffer capacitor is required. This worsens the power density and the converter efficiency. In the proposed converter, the boost inductor is utilized for both the boost operation and the active power decoupling operation by using DCM. In this paper, by harmonic analysis, the effectiveness of the active power decoupling method is evaluated. As a calculating result, the maximum power density of the proposed converter is 1.26 times higher than that of the passive topology. Especially, the boost inductor volume can be reduced by 42.7% applying by DCM. The fundamental operation is confirmed by a 1-kW prototype. From experimental results, a second-order harmonics on the input current is reduced by 90.2% with the proposed active power decoupling method. In addition, the maximum efficiency of 96.0% is achieved at the output power of 600 W.**

Keywords—High power density systems; Single phase system; Power decoupling;

I. INTRODUCTION

Recently, photovoltaic (PV) systems have been researched actively as a solution for sustainable power. Especially, the world PV market installation reached a high record of 277 GW in 2015 [1]. In order to utilize the generated power from the PV panels, power converter system (PCS) are employed in order to connect the PV system to the single-phase AC grid [2-3]. These PCS requires the following capabilities;

(1) High efficiency power conversion,

(2) “Plug-and-Play” operation,

(3) Maintenance-free,

(4) Small packaging design.

In order to satisfy these capabilities, a two-stage power conversion with a boost converter and a voltage source inverter (VSI) is employed due to its simple configuration in generally. Note that, the instantaneous power ripple component at twice grid frequency occurs owing to the single-phase AC grid. As a result, the performance of the maximum power point tracking (MPPT) decays. In order to absorb the power ripple component, a bulky electrolytic capacitor is employed in the DC-link in generally. However, the bulky electrolytic capacitor limits the life-time of the converter for PV systems according to Arrhenius law.

On the other hand, several circuit topologies with active power decoupling methods have been increasingly studied to eliminate the bulky electrolytic capacitor [4-15]. The active power decoupling methods can reduce the capacitance for the instantaneous power fluctuation compensation, which leads to the use of a film or a ceramic capacitor instead of the bulky electrolytic capacitor. However, the conventional active power decoupling methods decrease the converter efficiency due to the loss coming from the additional component. In particular, the additional magnetic component greatly introduces large volume.

In this paper, a novel active power decoupling topology which is constructed based on a boost converter is proposed. The proposed method does not require the additional magnetic component for the active power decoupling circuit, because the boost inductor is utilized for both the boost operation and the power decoupling capability applying by discontinuous current mode (DCM). Furthermore, an inductor applied to DCM can reduce the inductance [16]. Thus, the proposed topology can be further achieved the downsizing. In addition, the active power decoupling circuit can apply the low on-resistor switching device owing to the low voltage rating devices. Therefore, the proposed converter with DCM can achieve the high efficiency and the high power density. This paper is organized as follows; in section II, the proposed converter topology for the DC to single-phase AC converter are introduced. In section III, the principle of the active power decoupling is explained. In section IV, the control strategy of the proposed converter is explained. Finally, the validity of the proposed power decoupling is

confirmed by a 1-kW prototype in the experiment. The power density and the system efficiency of the each circuit topologies with the power decoupling capability are evaluated by Pareto-front optimization and the volume distribution.

II. Circuit Configuration

A. Conventional Circuit

Figure 1 shows a DC to single-phase AC grid-connected system with a typical boost converter. The boost converter pushes up the PV input voltage more than the peak voltage of the single-phase grid, and the generated power is supplied to the single-phase grid by the VSI. In this case, the bulky electrolytic capacitor C_{dc} is employed onto the DC-link in order to absorb the power ripple component which has twice grid frequency. If the power ripple component is absorbed by the bulky electrolytic capacitor at a DC link in the conventional system, the required capacitance is decided by the energy of the power ripple. Thus, the capacitor voltage ripple is expressed by

$$\Delta E = \frac{1}{2} C_{dc} \left\{ (V_{ave} + \frac{\Delta V_c}{2})^2 - (V_{ave} - \frac{\Delta V_c}{2})^2 \right\} \qquad (1),$$

where E is the energy of the power ripple caused by single-phase grid, V_{ave} is the average value of the bulky electrolytic capacitor voltage and ΔV_c is the fluctuation voltage of C_{dc}. In the conventional method with a bulky electrolytic capacitor as shown in Fig.1, ΔV_c is designed to be small for a stable operation of the inverter by using the large capacitance of C_{dc}. In this configuration, it is necessary to perform a periodic maintenance of the electrolytic capacitor owing to its short life-time.

Figure 2 shows a DC to single-phase AC grid-connected system. This system has a conventional active power decoupling circuit to compensate the power ripple. In this case, the DC-link capacitor value can be minimized in comparison with Fig. 1 because the power ripple is compensated by the small buffer capacitance of C_{buf}. Thus, the film or ceramic capacitor can be applied for the smoothing capacitor. As a result, the converter with the power decoupling circuit can be eliminated the bulky electrolytic capacitor. However, an additional magnetic component L_{buf} is required in order to control the buffer capacitor voltage V_{cbuf}. Consequently, this additional inductor increases the volume and the loss of the converter.

B. Proposed circuit

Figure 3 shows the proposed circuit which is constructed by an active power decoupling circuit based on the boost converter. This converter consists a boost converter, an H-bridge inverter and an active power decoupling circuit. Similar to the conventional active power decoupling circuit, the proposed converter can reduce the capacitance of the DC-link capacitor C_{dc} because the power ripple is compensated by the buffer capacitor C_{buf}. However, contrast to the conventional method,

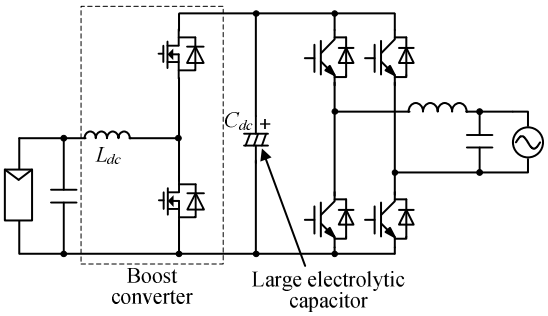

Fig. 1. Circuit configuration with typical boost converter. The bulky electrolytic capacitor C_{dc} is required for the compensation of the power ripple component in this circuit. As a result, the life-time of PCS is limited by C_{dc}.

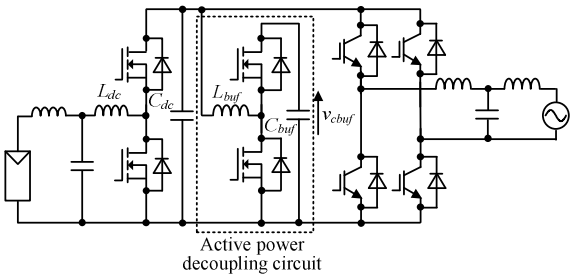

Fig. 2. Boost-type crircuit configuration with conventional active power decoupling circuit. C_{dc} can be reduced by the active power decoupling circuit. However, the additional magnetic component L_{buf} is required in order to control buffer capacitor voltage V_{cbuf}. Consequently, the converter loss and the volume of the converter increase due to L_{buf}.

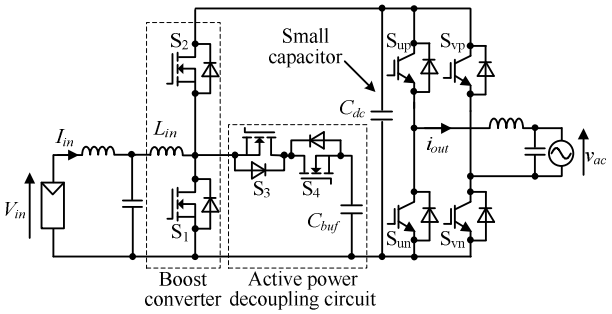

Fig. 3. Proposed converter with power decoupling capability. The boost inductor L_{in} is utilized for both the boost operation and the buffer capacitor voltage control for the power decoupling. Thus, the additional magnetic component is not required. The proposed converter is operated in DCM in order to discharge of C_{buf}.

the additional magnetic component L_{buf} as shown in Fig. 2 is not required for the active power decoupling circuit. This is because the boost inductor L_{in} is used in order to achieve the active power decoupling. Note that, in the active power decoupling circuit, a bidirectional switch is required for the prevention of the short-circuit between the DC link capacitor C_{dc} and the buffer capacitor C_{buf}. In particular, the active power decoupling circuit

performs the buck-type operation. Therefore, the voltage applied to this bidirectional switch is lower than the DC link voltage because the maximum value of this voltage is either the difference between the DC link voltage and the buffer capacitor voltage, or the low capacitor voltage. Therefore, low on-resistor switching device can be applied to S_3 and S_4 and the loss of S_3 and S_4 can be reduced to compare the boost-type active buffer circuit [17].

When the boost converter is operated in continuous current mode (CCM), the current pathway is limited in one direction. Therefore, with the application of CCM, the buffer capacitor control cannot perform both the charging mode and the discharging mode. In order to overcome this, the proposed converter is operated in the discontinuous current mode (DCM) in order to discharge the buffer capacitor C_{buf}. In particular, the buffer capacitor is discharged during the negative period of the inductor current on the DCM operation. In general, the inductor value applied with DCM can be reduced compared to CCM. Thus, the volume of the boost inductor is reduced by DCM.

III. Rrinciple of Power Decoupling Operation

Figure 4 depicts a principle of the power decoupling operation with the active buffer. When the output current has sinusoidal unity power factor, the instantaneous output power p_{out} is expressed by

$$\begin{aligned} p_{out} &= V_{acp}\sin(\omega t)\cdot I_{acp}\sin(\omega t) \\ &= \frac{V_{acp}I_{acp}}{2}(1-\cos 2\omega t) \end{aligned} \quad (2).$$

where V_{acp} is the single-phase grid voltage (peak), I_{acp} is the inverter output current (peak), and ω is the output angular frequency. As shown in (2), the power ripple, which has twice grid frequency, occurs at the DC-link. In order to compensate the power ripple at DC side, the instantaneous active buffer power p_{buf} should be controlled by

$$p_{buf} = -\frac{1}{2}V_{acp}I_{acp}\cos 2\omega t \quad (3)$$

where the polarity of instantaneous power of an active buffer is define as positive when the active buffer discharges. When the power decoupling is applied, the input power p_{in} is matched to the average value of p_{out}.

$$p_{in} = \frac{1}{2}V_{acp}I_{acp} = V_{in}I_{in} \quad (4)$$

IV. Control Strategy of Proposed Circuit

A. Control strategy

Figure 5 illustrates the operation mode of the proposed converter which has four modes. Mode 1 and Mode 2 are the

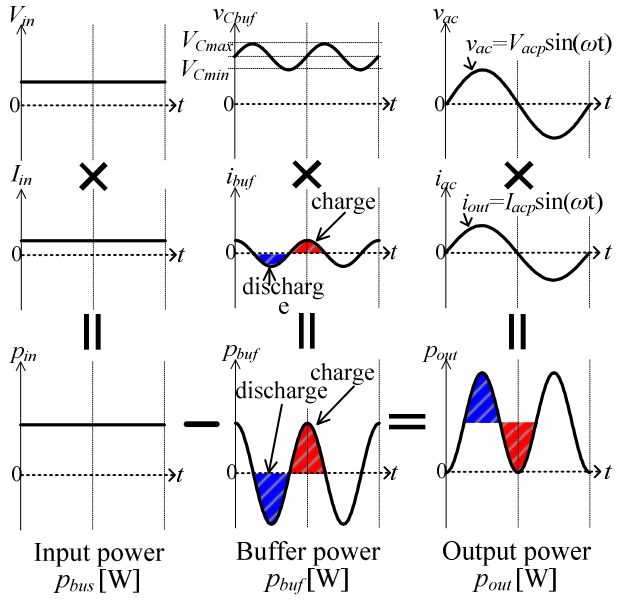

Fig. 4 Principle of power decoupling. The buffer power to absorb the power ripple component is charged/discharged by the buffer capacitor. Consequently, the DC current without the power ripple is obtained.

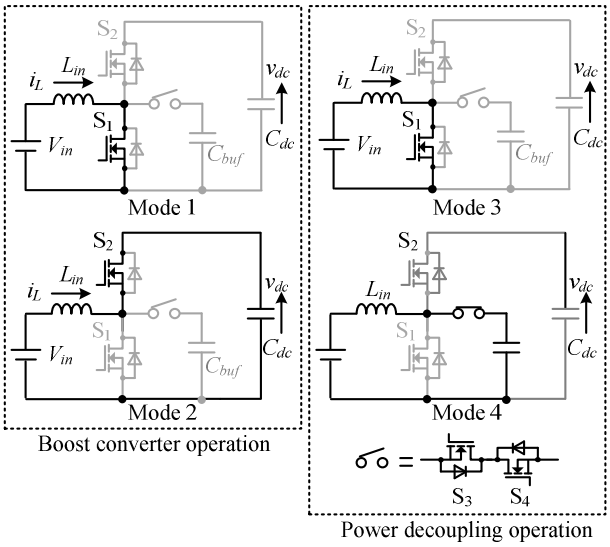

Fig. 5. Operation mode of proposed converter. The proposed converter achieves the boost operation and the active power decoupling operation through four modes.

boost operation, where the PV input voltage V_{in} is pushed up to the DC link voltage V_{dc} higher than V_{acp}. Note that, S_3 and S_4 is always off in order to separate the power decoupling operation from the boost operation. In Mode 3 and Mode 4, the buffer capacitor is charged and discharged for the compensation of the power ripple component.

Figure 6 shows the control block diagram of the proposed converter which consists of the buffer capacitor voltage control and the DC link voltage control. The current and voltage control in the proposed method are implemented by PI controller. The DC link voltage is regulated more than the peak grid voltage by the voltage control (AVR). Equally, the buffer capacitor voltage is fluctuated at twice grid frequency for the active power decoupling. If the fluctuation of the buffer capacitor voltage is controlled by a voltage controller (AVR), the bandwidth of the AVR has to be high. This can be avoided by regulating only the average voltage by the AVR in the buffer capacitor voltage control. Meanwhile, the charge and discharge value of the buffer capacitor is controlled by the boost inductor current control (ACR).

Figure 7 shows the boost inductor current waveforms in DCM. In order to separate the DC-link voltage control from the buffer capacitor voltage control, the zero-current period is inserted into each current mode.

Note that, in order to achieve the proposed active power decoupling, the boost inductor average current i_{L_ave}, which is the sum of the DC link current and the buffer capacitor current, has to become constant.

The boost inductor current is expressed as

$$i_{L\_ave} = i_{L\_ave\_dc} + i_{L\_ave\_buf} \tag{5}$$

where $i_{L\_ave\_dc}$ is the DC link average current, $i_{L\_ave\_buf}$ is the buffer capacitor average current.

On the other hand, the DC link average current $i_{L\_ave\_dc}$ is expressed as

$$i_{L\_ave\_dc} = \frac{i_{peak}}{2}(d_1 + d_2) = \frac{P_{out}}{V_{in}}[1 - \cos(2\omega t)] \tag{6}$$

where d_1 and d_2 are the duty reference of mode 1 and mode 2, P_{out} is the output power. When the active power decoupling is not applied, the inductor average current is fluctuated at twice grid frequency as shown in (6). In order to obtain the constant current by the power decoupling, the buffer capacitor current has to be fluctuate in order to compensate the power ripple component.

When the active power decoupling is applied, the buffer capacitor average current $i_{L\_ave\_buf}$ is expressed as

$$i_{L\_ave\_buf} = \frac{i_{peak}}{2}(d_3 + d_4) = \frac{P_{out}}{V_{in}}\cos(2\omega t) \tag{7}$$

where d_3 and d_4 are the duty reference of mode 3 and mode 4. According to (6) and (7), the boost inductor average current i_{L_ave} becomes constant, and the buffer capacitor voltage is

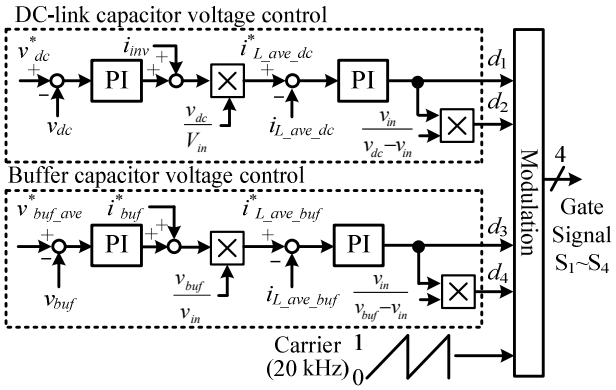

Fig. 6. Control block diagram of proposed converter.

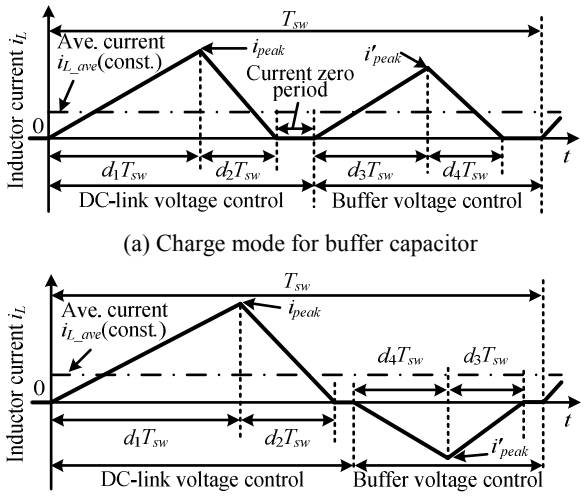

(a) Charge mode for buffer capacitor

(b) Discharge mode for buffer capacitor

Fig. 7. Current waveform of boost inductor with DCM for active power decoupling circuit.

fluctuated at twice grid frequency owing to the proposed control. Thus, the proposed converter does not required the additional magnetic component for the active power decoupling.

B. Designing method of boost inductor

In Figure 7 (b), in order to prevent an interference between the two voltage control loops, each duties necessary to meet the equation (8).

$$d_1 + d_2 + d_3 + d_4 \le 1 \tag{8}$$

When the sum of each duty is equal to 1, the operation mode of this proposed is the CCM. The current ripple of the boost inductor becomes the minimum, which leads to the minimum of the conduction loss in the critical condition. Thus, the inductance of the boost inductor L_{in} is designed based on the critical condition at the rated power, and is calculated by

$$L_{in} = \frac{V_{in}^2(\alpha_{di}-1)}{4 f_{sw} P_{out} \alpha_{di}\left(1+\sqrt{\frac{\alpha_{bd}}{2}\frac{\alpha_{di}-1}{\alpha_{di}\alpha_{bd}-1}}\right)^2} \quad (9)$$

$$\alpha_{di} = \frac{V_{dc}}{V_{in}} \quad (10)$$

$$\alpha_{bd} = \frac{V_{buf\_ave}}{V_{dc}} \quad (11)$$

where f_{sw} is the switching frequency, α_{di} is the boost ratio of the DC-link voltage to V_{in}, α_{bd} is the boost ratio of the average voltage of C_{buf} to the DC-link voltage, and V_{buf_ave} is the average voltage of C_{buf}.

V. Simulation and Experimental Results

A. Simulation Results in Steady State

Table I presents a simulation conditions in order to verify the fundamental operation of the proposed converter with the active buffer. Note that the output voltage is 100 V_{rms}, the dead time and the input filter is not replaced for simplicity. In order to remove a switching ripple, the boost inductor current is filtered with a LPF with the cut-off frequency of 2 kHz.

Figure 8 shows the input and output waveforms of the proposed converter. Fig. 8 (a) shows a result without the proposed active power decoupling. As shown in Fig. 8 (a), the boost inductor current is distorted by the power ripple component. This cause is the proposed circuit has a small capacitance of C_{buf} which is not completely compensated the power ripple at 100 Hz. In contrast, Fig. 8 (b) shows a result with the power decoupling. The power ripple component is reduced in Fig. 8 (b), owing to the proposed active power decoupling.

Figure 9 shows extended waveforms of area A and area B in Fig.8. Fig. 9 (a) shows the charging mode with the buffer capacitor, whereas Fig. 9 (b) shows the discharging mode of the buffer capacitor. The boost inductor current becomes discontinuous, i.e. DCM. As shown in Fig. 9 (a), the first current ripple as a smaller side performs the operation, whereas the secondary current ripple as a bigger side performs the active power decoupling, i.e. the charge mode of the buffer capacitor. Similarly, as shown in Fig. 9 (b), the positive performs the boost operation, whereas the negative current ripple performs the active power decoupling, i.e. the discharge mode of the buffer capacitor. The boost current ripple Therefore, the proposed active power decoupling compensates the power ripple component on the input current without any additional magnetic component.

B. Experimantal results in Steady State

In order to evaluate the fundamental operation, a 1-kW prototype circuit is tested. It should be noted that the

Table I. Simulation and experimental condition.

Output power	P_{out}	1 kW
Output frequency	f_{out}	50 Hz
Input voltage	V_{in}	150 V
Switching frequency	f_{sw}	20 kHz (VSI : 10 kHz)
Buffer capacitor	C_{buf}	80 μF
Boost-up inductor	L_{in}	48 μH
Input filter cut-off frequency	f_{filter}	2 kHz
DC link capacitor	C_{dc}	54 μF
Load		R-L load

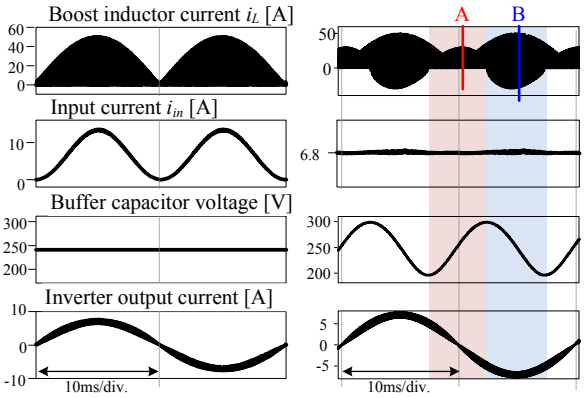

(a) W/o active power decoupling (b) With active power decoupling

Fig. 8. Fundamental operation waveforms. The boost current waveform with DCM is deiced by the mode of the buffer capacitor voltage.

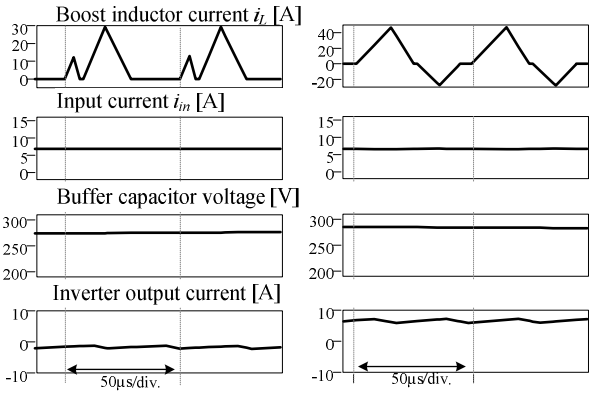

(a) Area A of Fig. 8 (b) Area of Fig. 8

Fig. 9. Extended current waveform of area A and B in Fig. 8 with power decoupling method using DCM. This figure shows the buffer capacitor in the charging mode as shown in area A and the discharging mode as shown in area B of Fig. 8.

experimental condition is similar table I. In this paper, instead of the grid-connection, the RL load is employed. However, the occurrence of the instantaneous power ripple at the twice grid frequency is still the same. In this experiment, the buffer capacitor value of 80 μF, the DC link capacitor of 54 μF, and the boost inductor of 48 μH are employed.

1) Fundamental operation

Figure 10 shows the experimental result without the proposed active power decoupling. As shown in Fig. 10, the buffer capacitor voltage is constant. Therefore, the input current i_{in} fluctuates at twice grid frequency due to the power ripple component. In this result, the ripple component in the input current i_{in} is 54.7% with reference to the average input current.

Figure 11 shows the experimental result with the proposed active power decoupling. In comparison with Fig. 10, the input current i_{in} becomes almost constant. The ripple component in the input current at 100 Hz is 5.36% with reference to the average input current. Moreover, the buffer capacitor voltage is fluctuated at the twice grid frequency to absorb the power ripple.

It is also confirmed that the inverter output current becomes sinusoidal which has low distortion. From these results, the proposed active power decoupling with a buffer capacitor of 80 μF is achieved.

Figure 12 shows the harmonic analysis of the boost inductor current. Note that the harmonic number is based on the grid frequency of 50 Hz and boost inductor current is based on the 100 Hz component of the boost inductor current. The proposed active power decoupling method reduces the 2nd-order harmonics (100 Hz) by 90.2% in comparison with no adopting the proposed active power decoupling. From this result, the validity of the proposed converter with the power decoupling capability is confirmed without the additional magnetic component for the proposed circuit.

Figure 13 shows the efficiency system characteristics of the proposed converter when the active power decoupling is applied. The maximum efficiency reaches 96.0% at the output power of 600 W. In order to achieve the high power density, the low on-resistor switching devices could be applied into the active power decoupling circuit in the proposed inverter. As shown in Fig.13, the proposed inverter using the buck-type active buffer is confirmed an improvement in the switching loss of the buffer circuit compared to the proposed inverter using the boost-type active buffer [17].

2) Volume evaluation

a) Comparison of Pareto-front for DC-DC converter

The fundamental operation and the active power decoupling capability of the proposed inverter using the buck-type active buffer are confirmed in the previous section. In order to confirm the converter efficiency and the power density of the proposed

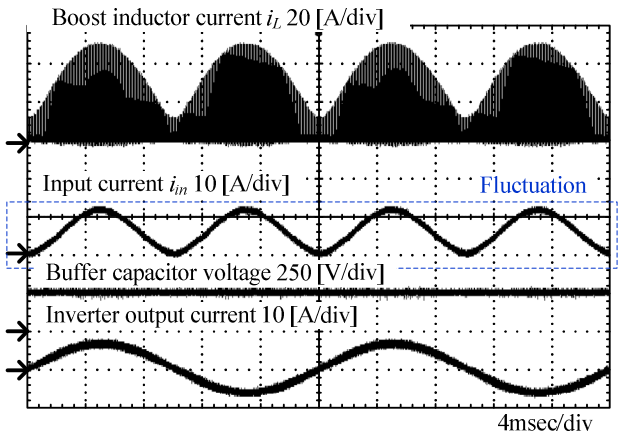

Fig. 10. Experimental result without active power decoupling. The input current i_{in} fluctuates at twice grid frequency.

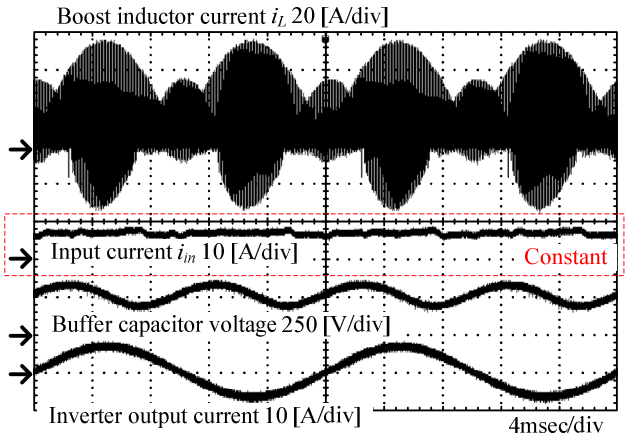

Fig. 11. Experimental result with active power decoupling. The input current i_{in} becomes constant, and the buffer capacitor voltage is fluctuated at twice grid frequency.

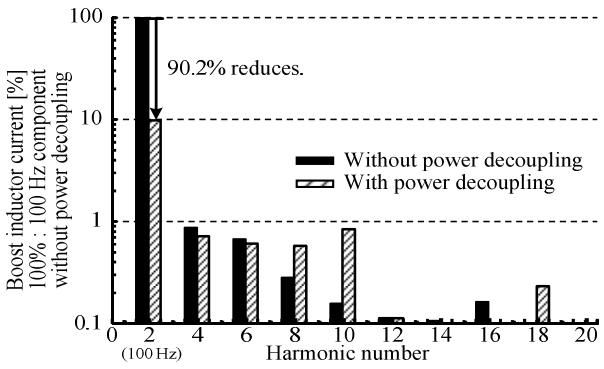

Fig. 12. Harmonic analysis of boost inductor current. The active power decoupling method reduces the second-order harmonics of the power ripple component by 90.2%.

inverter with DCM, the each converter topologies are compared using the pareto-front optimization.

Figure 14 shows the pareto-front of the power density and the converter efficiency at the range of the switching frequency from 1 kHz to 100 kHz.

Table II presents the selected components. In particular, the power density ρ_{power} is calculated from the total volume Vol_{total} by (12)-(13). Moreover, the efficiency η of the each converters is provided by (14).

$$\rho_{power} = \frac{P_{out}}{Vol_{total}} \tag{12}$$

$$Vol_{total} = Vol_{Lbuf} + Vol_{Cbuf} + Vol_{sw} + Vol_{heatsink} \tag{13}$$

$$\eta = \frac{P_{out}}{P_{out} + \left(P_{loss} + P_{loss\_Cbuf} + P_{loss\_Cdc}\right)} \tag{14}$$

where Vol_{Cbuf} is volume of C_{buf} and Vol_{sw} is the volume the package of the switching device. $Vol_{heatsink}$ is the volume of the cooling system, Vol_{Lbuf} is volumes of the buffer inductor or the boost inductor. P_{loss} is the sum of the conduction loss and switching loss. P_{loss_cbuf} and P_{loss_cdc} are the loss of the buffer capacitor and the DC link capacitor C_{dc}. These parameter of (12)-(14) is calculated by reference from [17-21]. The power density ρ_{power} reaches the maximum value at the range of the switching frequency from 1 kHz to 100 kHz. Note that Fig. 14 shows a calculation result, when the components as shown in table II is used in the each converters with the power decoupling circuit. In particular, in the proposed converter, the maximum power density of 7.2 kW/dm^3 is achieved with the efficiency of 98.6%. In contrast, in the passive topology, maximum power density of 5.7 kW/dm^3 is achieved with the efficiency of 98.8%. Thus, the proposed system with DCM is 1.26 times higher than the passive topology.

b) Comparison of each volumes

Figure 15 shows the volume ratio of DC-DC converters with the power decoupling capability at the maximum power density point as shown in Fig. 14. The components volume is normalized with the volume of the bulky electrolytic capacitors of the passive topology as 100%. In the conventional buck-type converter reduces the volume of the buffer capacitor by 74.3% compared to the bulky electrolytic capacitors in the passive topology. However, $Vol_{heatsink}$ and Vol_{sw}, and the volume of the boost inductor are 61.0% and 42.2% compared to the passive topology, respectively. The boost inductor size can be reduced by increasing the switching frequency in generally. However, the cooling system size increases due to the increase of the switching loss. Thus, the conditional active buffer method be achieved the downsizing of the smoothing capacitor as a C_{buf} while at the same time increasing the volume of the active buffer

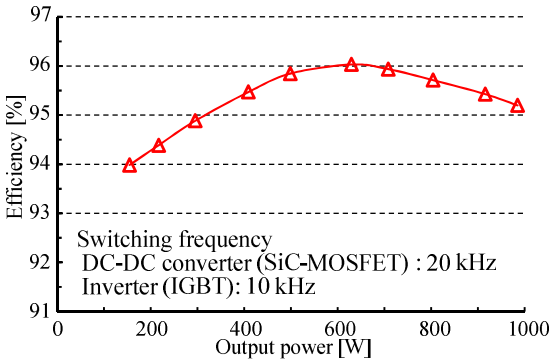

Fig. 13. Efficiency characteristics of proposed converter. The maximum efficiency is 96.0% when output power is 600 W.

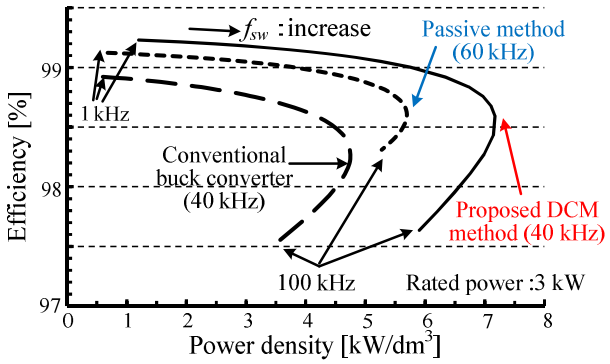

Fig.14. Pareto-front of DC-DC converter with active power decoupling capability. The proposed converter using the buck-type active buffer topology is achieved the maximum power density at 40 kHz of the switching frequency.

circuit. In contrast, the proposed converter reduces the buffer capacitor size by 48.7% compared to bulky electrolytic capacitors in the passive topology. Moreover, in proposed converter with active power decoupling, the sum of $Vol_{heatsink}$ and Vol_{Lbuf} are reduced by 47.5% and 42.7% compared to the conventional buck-type converter.

VI. Conclusiton

This paper proposed a novel active power decoupling topology based on the boost converter without any additional magnetic component. The proposed converter utilized the boost inductor for both the boost operation and the buffer capacitor voltage control. In addition, the power decoupling circuit performs the buck-type operation, and the low on-resistor switching device could be applied into the active power decoupling circuit. Thus, the conduction loss could become small. As the experimental result, the proposed active power decoupling method reduced the power ripple component at 100 Hz on the input current i_{in} by 90.2%. In addition, the maximum system efficiency of 96.0% was achieved at the output power of

Table II. Selected components.

Circuit topology	Part	Marking	Maximum ration
Passive	C_{in}	Nippon Chemi-Con EKMZ451VSN181MP30S	450 V 1.0 Arms 180 μF
Step down type active buffer	C_{buf}	Murata Manufacturing EVS20329S2G306MS09	400 V 30 μF
	SW1 SW2	ROHM SCT2120AF	650 V 29 A
Buck type active buffer with DCM	C_{buf}	Murata Manufacturing EVS20329S2G306MS09	400 V 30 μF
	SW1 SW2 SW3 SW4	ROHM SCT3017AL	650 V 60 A

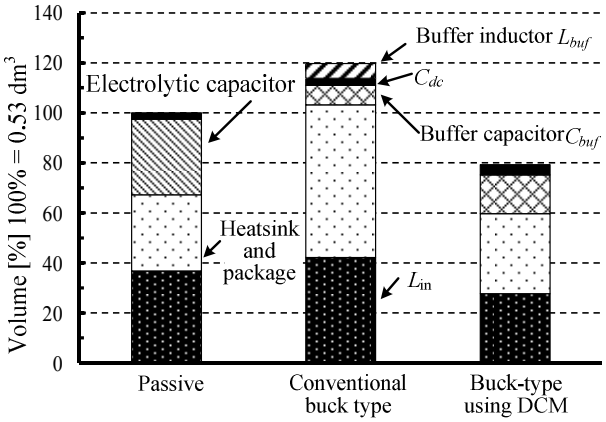

Fig.15. Volume distribution of DC-DC converter. The volume of the proposed converter with DCM is 0.42 dm^3.

600 W. In addition, the total components volume of the DC-DC converter in the proposed topology was less than 20.7% compared to the passive topology. Especially, the boost inductor volume can be reduced by 42.7% using DCM. Thus, the validity of the proposed converter with the active power decoupling was confirmed.

REFERENCES

[1] International Energy Agency Photovoltaic Power systems Programme annual report 2015 (2015)

[2] Suroso, T. Noguchi "Three-Level Current Source PWM Inverter with No Isolated Switching Devices for Photovoltaic Conditioner" IEEJ trans., No.5, pp. 505-510 (2009)

[3] J. Leppaaho, J. Huusari, L. Nousiainnen, J. Puukko, T. Suntio "Dynamic Properties and Stability Assessment of Current-Fed Converter in Photovoltaic Applications" IEEJ trans., No.8, pp. 976-984 (2011)

[4] S. Qin, Y. Lei, C. Barth, W. Liu, R. C. N. Pilawa-Podgurski : "A High-Efficiency High Energy Density Buffer Architecture for Power Pulsation Decoupling in Grid-Interfaced Converters", IEEE ECCE 2015, pp.149-157 (2015)

[5] C. B. Barth, I. Moon, Y. Lei, S. Qin, R. C. N. Pilawa-Podgurski: "Experimental Evaluation of Capacitors for Power Buffering in Single-Phase Power Converters", ECCE 2015, pp. 6269-6276 (2015)

[6] Montie. A, Luciano. F.S Alves, Ruxi. Wang, and Mauricio. B.R. Correa, "Low-Frequency Power Decoupling in Single-Phase Applications overview,"IEEE Transactions on Power Electronics, vol: pp. (2016)

[7] S. Kjaer and J. Pedersen, "A review of single-phase grid-connected inverters for photo-voltaic modules," IEEE Trans. Ind. Ap., vol. 41, no. 5, pp. 1292-1306, (2005)

[8] Siyuan Ma, Haoran Wang, Hunchaojie Tang, Guorong Zhu and Huai Wang "Lifetime estimation of DC-link capacitors in a single-phase converter with an integrated active power decoupling module" IECON 2016, pp. 6824-6829 (2016)

[9] V.V.S. Pradeeo Kumar, B.G. Fenabdes "transformerless active power decoupling topologies for grid connected PV applications" IECON 2016, pp. 2410-2419 (2016)

[10] Ioan Serban, Comeliu Marinescu, Daniel Munteanu "Performance analysis of a SiC-based single-phase H-bridge inverter with active power decoupling" EPE 2016 pp.1-10 (2016)

[11] Yao Sun, Yinglu Liu, Xin Li, Jian Yang "Active power decoupling method for single-phase current source rectifier with no additional active switches" IEEE trans. vol. 31, pp.5644-5654 (2016)

[12] Yi Tang, Frede Blaabjerg, "An efficiency improved active power decoupling circuit with minimized implementation cost" 2014 international power electronics and application conference and exposition. pp. 864-869 (2014)

[13] Nataraj Pragallapati, Vivek Agarwal, "Single phase solar PV module integrated flyback based micro-inverter with novel active power decoupling" PEMD 2014. pp. (2014)

[14] Wenlong Qi, Hui Wang, Xingguo Tan, Guangzhu Wang, Khai D.T Ngo, "A novel active power decoupling single-phase PWM rectifier topology" APEC 2014. pp. 89-95 (2014)

[15] T. Hirao, T. Shimizu, M. Ishikawa, K. Yasui "Discussion on Modulation Methods for Flyback-type Single-phase Inve rters with Enhanced Power Decoupling for Photovoltaic AC module Systems" IEEJ trans., No.4, pp. 504-510 (2006)

[16] Le Hoai Nam, Koji Orikawa, Jun-ichi Itoh : "DCM Control Method of Boost Converter based on Conventional CCM Control", The 2014 International Power Electronics Conference , No. 21A4-5, pp. 3661-3666 (2014)

[17] J. Itoh, T. Sakuraba, H. N. Le, K. Kusaka: "Requirements for Circuit Components of Single-Phase Inverter Applied with Power Decoupling Capability toward High Power Density", 18th European Conference on Power Electronics and Applications (EPE'16), No. DS2a 0291, (2016)

[18] S. Qin, Y. Lei, C. Barth, W. Liu, R. C. N. Pilawa-Podgurski : "A High-Efficiency High Energy Density Buffer Architecture for Power Pulsation Decoupling in Grid-Interfaced Converters", IEEE ECCE 2015, pp.149-157 (2015)

[19] Wm. T. Mclyman : "Transformer and inductor design handbook", Marcel Dekker Inc., (2004)

[20] U. Drofenik, G. Laimer and J. W. Kolar : "Theoretical Converter Power Density Limits for Forced Convection Cooling", Proceedings of the International PCIM Europe Conference, pp. 608-619 (2005)

[21] T. Nakanishi and J. Itoh, "Capacitor volume evaluation based on ripple current in Modular Multilevel Converter", International Conference on Power Electronics, No. 09, pp. 815-822(2015)